Supplementary Fig. S1

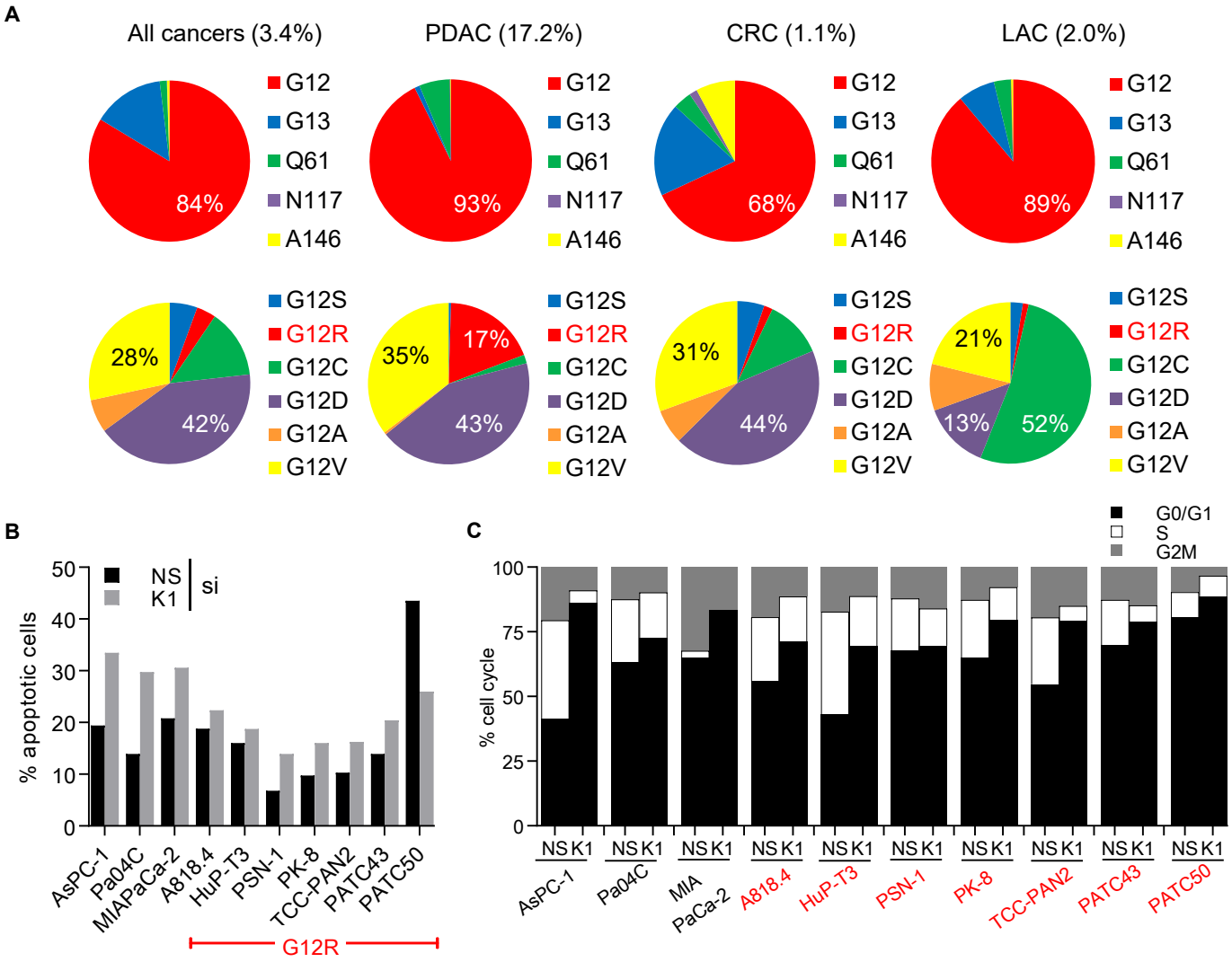

Figure S1. KRAS^{G12R} is the third most prevalent mutation in PDAC.
A, KRAS mutation frequency in PDAC, CRC and LAC. The top row provides the mutational frequency by amino acid position, and the bottom row provides the prevalence of G12 mutations in each cancer. **B,** Apoptosis assays of siRNA-transfected PDAC cells measured by Annexin V-FITC staining. Data are representative of two independent experiments. **C**, Cell cycle analyses of siRNA-transfected PDAC cells determined by staining with propidium iodide. At least 10^4 cells were collected for apoptosis and cell cycle assays, and data are representative of at least two independent experiments. Error bars, mean ± s.e.m.

Supplementary Fig. S2

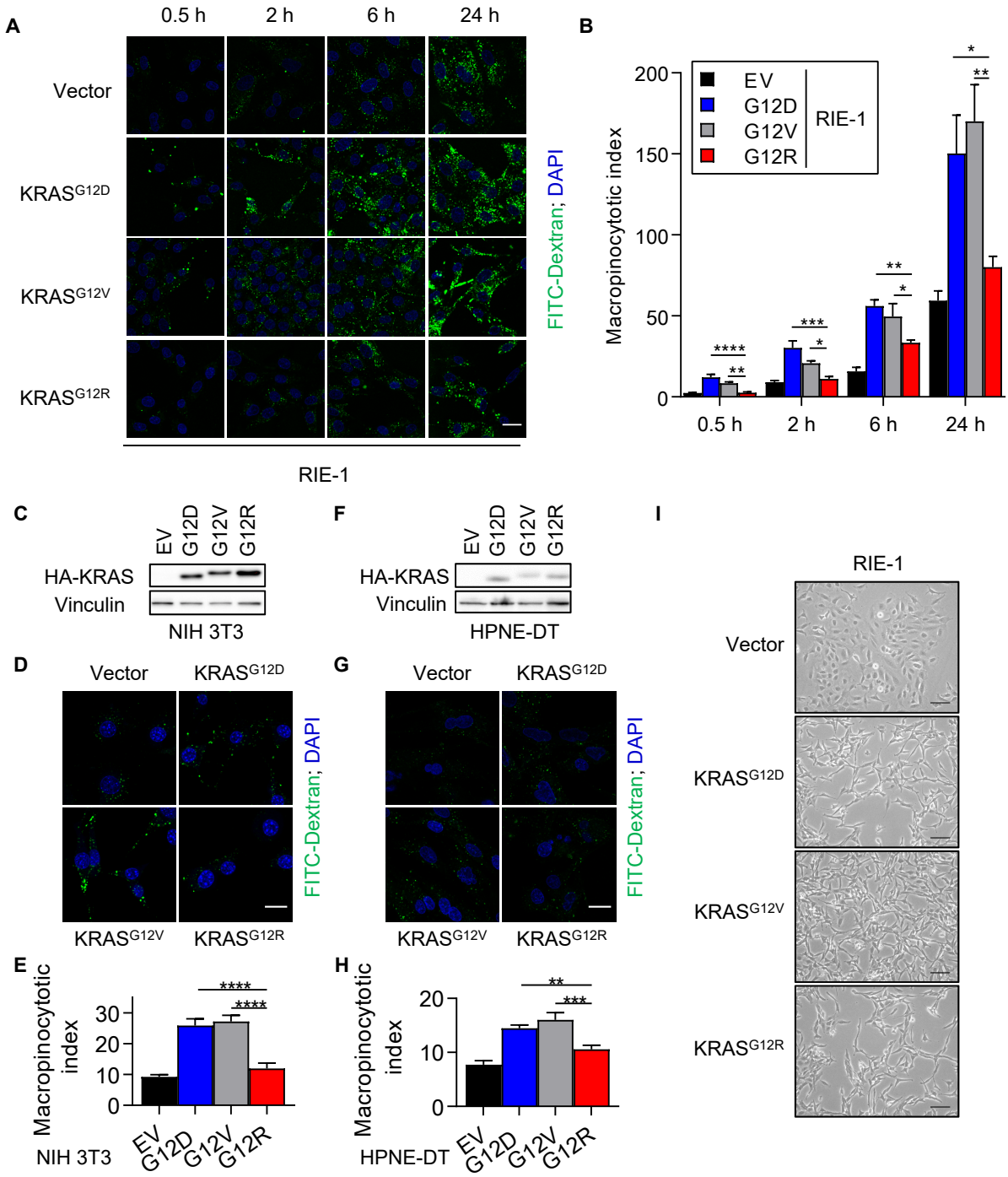

Figure S2. Ectopic expression of KRAS^{G12D} and KRAS^{G12V} mutants elevate macropinocytosis in model systems.

A, Time-dependent measurement of FITC-dextran labeled macropinosomes in KRAS-transformed RIE-1 cells. Macropinosomes, green; nuclei, blue, for the indicated time. Assay used 1 ml of 1:20 FITC-dextran/DMEM. **B**, Quantification of macropinocytosis index. Quantification performed with at least 50 cells per condition, and data are representative of two independent experiments. **C**, Immunoblot analysis of HA epitope-tagged KRAS expression levels in NIH/3T3 cells. **D,** FITC-dextran labeled macropinosomes in KRAS-transformed NIH/3T3 cells. **E**, Quantification of macropinocytotic index. Quantification of macropinocytosis index with at least 50 cells per condition, and data are representative of two independent experiments. **F**, Immunoblot analysis of HA epitope-tagged KRAS expression levels in HPNE-DT cells. G**,** FITC-dextran labeled macropinosomes in KRAS-transformed HPNE-DT cells. **H**, Quantification of macropinocytotic index. Quantification of macropinocytosis index with at least 50 cells per condition, and data are representative of three independent experiments. **I**, Brightfield microscopy images of RIE-1 cells transfected with KRAS mutants. Scale bar, 100 μm. For all data; ****P<0.0001, ***P<0.0002, **P<0.0021, *P<0.032, p values from Dunnett's multiple comparison test after one-way ANOVA, comparing all lanes to G12R at each time point. Scale bar is 20 μm, unless otherwise noted. Error bars, mean ± s.e.m.

Supplementary Fig. S3

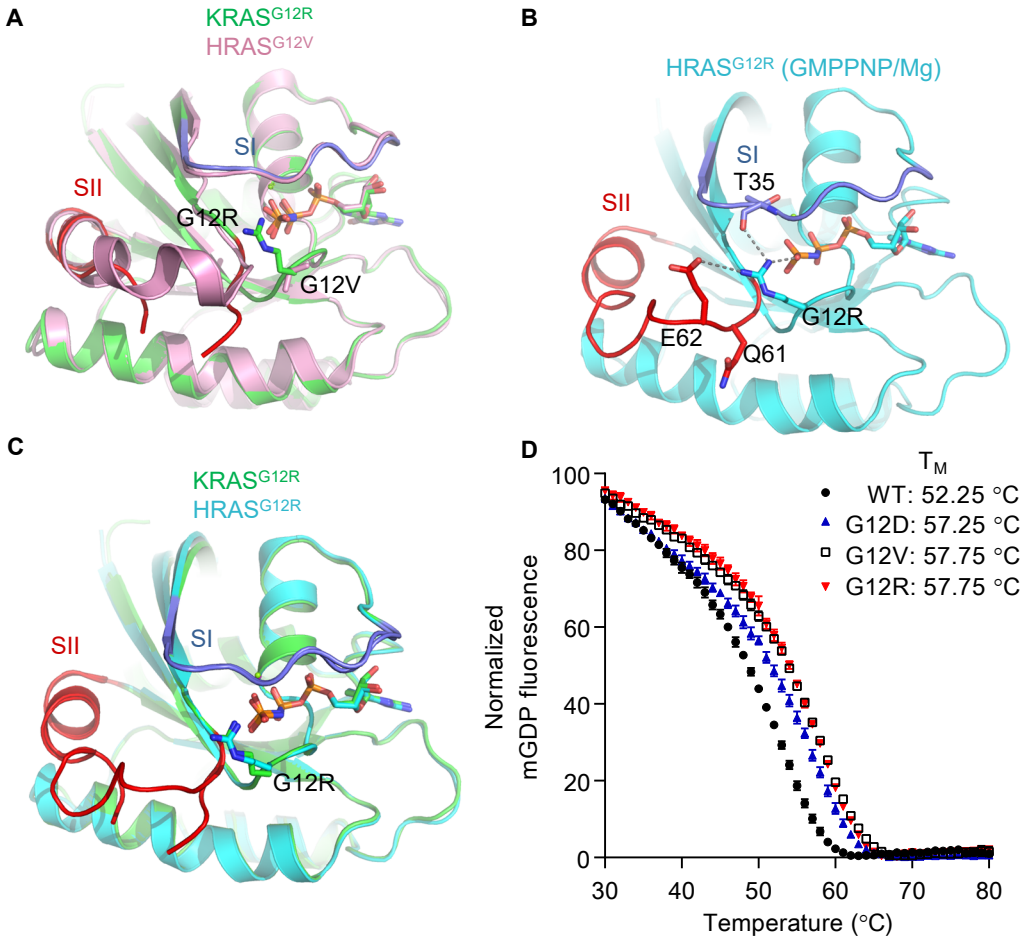

Figure S3. KRAS^{G12R} structure is unique among G12 mutations.
A, Overlay of the ribbon diagrams of KRAS^{G12R} (green) and HRAS^{G12V} (pink; PDB 3OIW). SI, light blue; SII, red. Stick models of G12V and G12R are shown. GMPPNP is shown with phosphates colored orange. **B**, A ribbon diagram of the HRAS^{G12R} crystal structure with selected side chains represented as sticks. Carbons in Q61 and E62 are colored red, nitrogen is blue and oxygen light red. T35 carbons colored in light blue. Hydrogen bonds are shown as gray dashed lines. **C**, Overlay of the ribbon diagrams of HRAS^{G12R} (teal) with KRAS^{G12R} (green). All other coloring is the same as previous. **D**, Thermal denaturation of KRAS proteins as measured by mGDP binding.

Supplementary Fig. S4

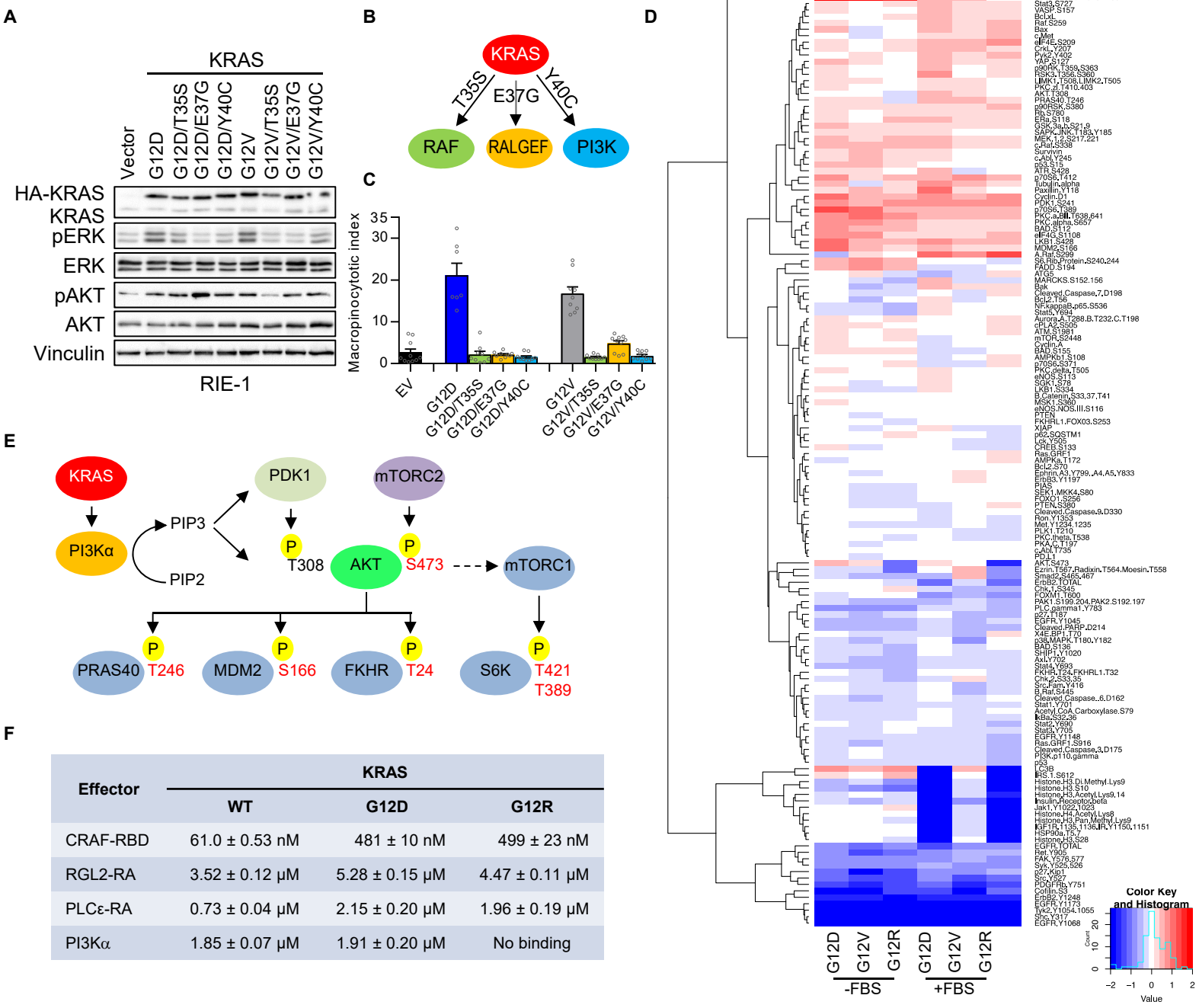

F

Effector	KRAS		
	WT	G12D	G12R
CRAF-RBD	61.0 ± 0.53 nM	481 ± 10 nM	499 ± 23 nM
RGL2-RA	3.52 ± 0.12 μM	5.28 ± 0.15 μM	4.47 ± 0.11 μM
PLCε-RA	0.73 ± 0.04 μM	2.15 ± 0.20 μM	1.96 ± 0.19 μM
PI3Kα	1.85 ± 0.07 μM	1.91 ± 0.20 μM	No binding

Figure S4. KRAS^{G12R} does not interact with p110α/p85 in vitro and in RIE-1 cells.
A, Immunoblot analysis of RIE-1 cells transfected with HA epitope-tagged KRAS effector-specific mutants. Vinculin was used a total lysate control, and phospho-specific and total AKT and ERK levels were probed. **B,** A diagram of the expected signaling preference for the KRAS effector-specific mutants. **C**, Quantification of macropinocytosis in KRAS effector-specific mutants with at least 50 cells per condition, and data are representative of two independent experiments. Error bars, mean ± s.e.m. **D,** Heatmap of the relative RPPA intensity of 162 proteins in RIE-1 cells ectopically expressing KRAS mutants cultured in the absence or presence of serum. **E**, KRAS-PI3K effector signaling diagram displaying the expected phosphorylation sites downstream of PI3K activation in cells. **F**, Table of KRAS WT and mutant protein binding affinities to select effector RBD/RA domains and full length p110α/p85. Values were determined using the inhibition of nucleotide dissociation assay as described. All experiments were performed in triplicate or greater, and the results are the average binding affinity.

Supplementary Fig. S5

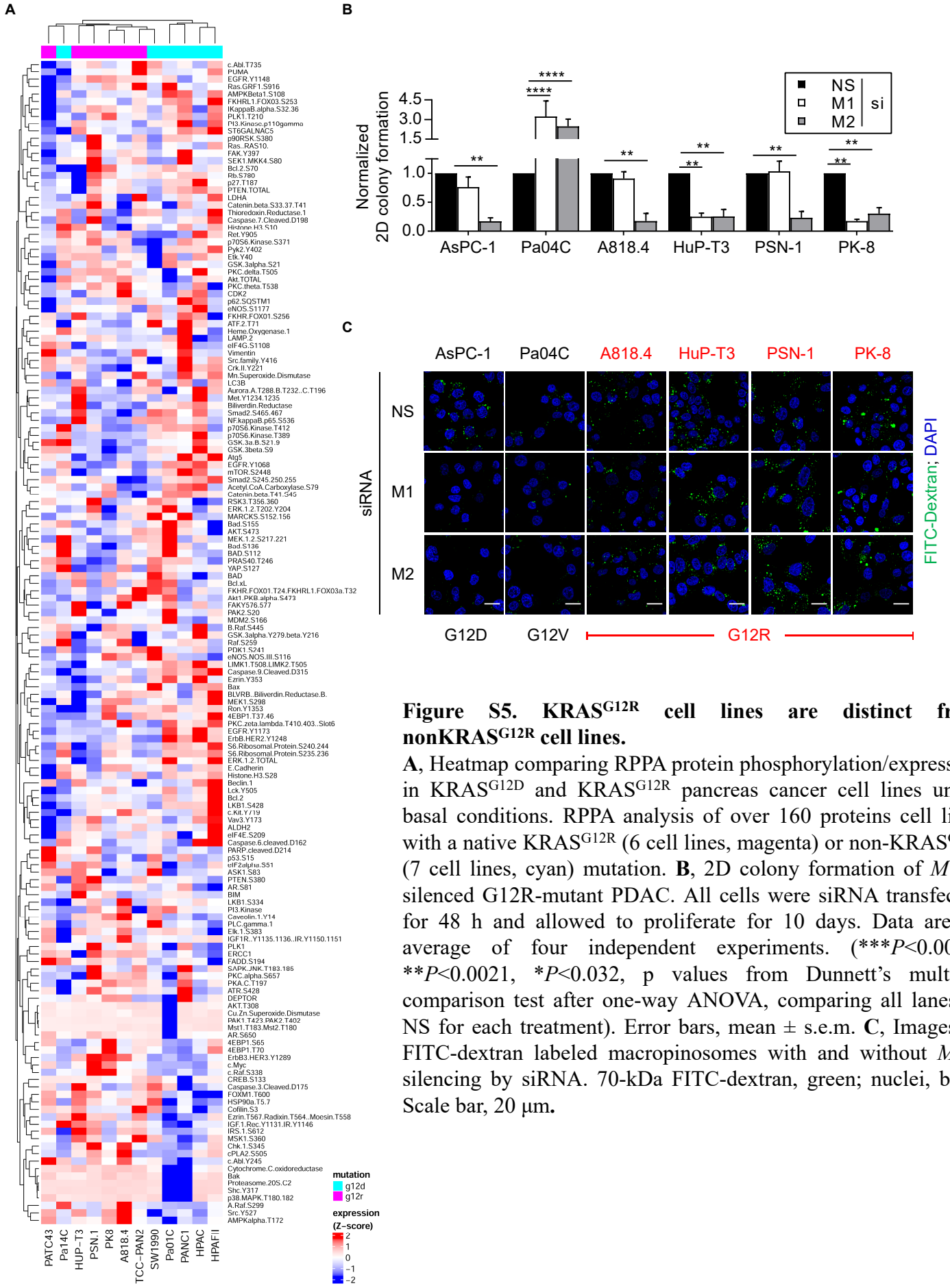

Figure S5. KRAS^{G12R} cell lines are distinct from nonKRAS^{G12R} cell lines.

A, Heatmap comparing RPPA protein phosphorylation/expression in KRAS^{G12D} and KRAS^{G12R} pancreas cancer cell lines under basal conditions. RPPA analysis of over 160 proteins cell lines with a native KRAS^{G12R} (6 cell lines, magenta) or non-KRAS^{G12R} (7 cell lines, cyan) mutation. **B**, 2D colony formation of *MYC*-silenced G12R-mutant PDAC. All cells were siRNA transfected for 48 h and allowed to proliferate for 10 days. Data are an average of four independent experiments. (***P<0.0002, **P<0.0021, *P<0.032, p values from Dunnett's multiple comparison test after one-way ANOVA, comparing all lanes to NS for each treatment). Error bars, mean ± s.e.m. **C**, Images of FITC-dextran labeled macropinosomes with and without *MYC* silencing by siRNA. 70-kDa FITC-dextran, green; nuclei, blue. Scale bar, 20 μm.

Supplementary Fig. S6

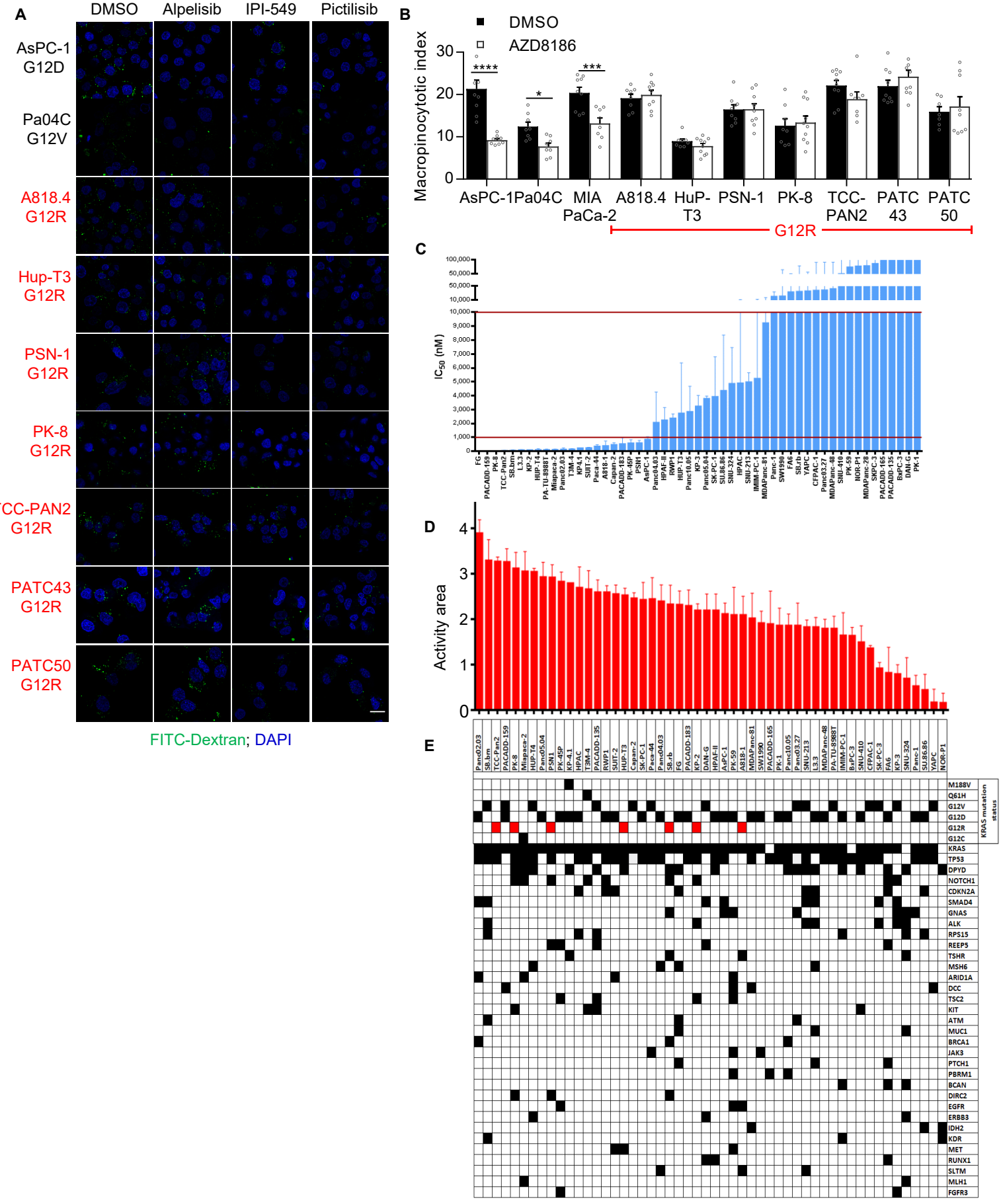

Figure S6. $KRAS^{G12R}$-mutant PDAC rely on p110γ for macropinocytosis and are sensitive to MEK/ERK inhibition.

A, Images of FITC-dextran labeled macropinosomes of PDAC cell lines treated for 24 h with DMSO, alpelisib (p110α-selective inhibitor, 100 nM), IPI-549 (p110γ-selective inhibitor, 300 nM) or pictilisib (pan-p110 inhibitor, 1.5 μM) for 18 hrs. Images are representative from four independent experiments. **B**, Quantification of FITC-dextran labeled macropinosomes in PDAC cell lines treated for 18 h with DMSO or AZD8186 alpelisib (p110α/β/δ-selective inhibitor, 1.0 μM). **C**, Response to selumetinib (AZD6244) measured by IC_{50} values (in nM) in a pancreas cancer cell line panel. The most sensitive cell line is shown on the left (N≥3 with SEMs; in triplicate). **D**, Response to selumetinib measured by the activity area. Activity area in 52 PDAC cell lines derived from 10-concentration dose response curves (N≥3 per cell line; in triplicate). Average Activity area (AA), as a measurement of maximum response and potency, aligned with *KRAS* mutation information from COSMIC (if available). AA integrates potency (EC_{50} or IC_{50}) and maximum response (A_{max}) at the highest drug concentration. **E,** Genetic mutations in 52 pancreatic cancer cell lines. The 250 most common cancer genes afflicted by somatic mutations were sequenced and genes with mutations found in at least two cell lines are shown

Supplementary Fig. S7

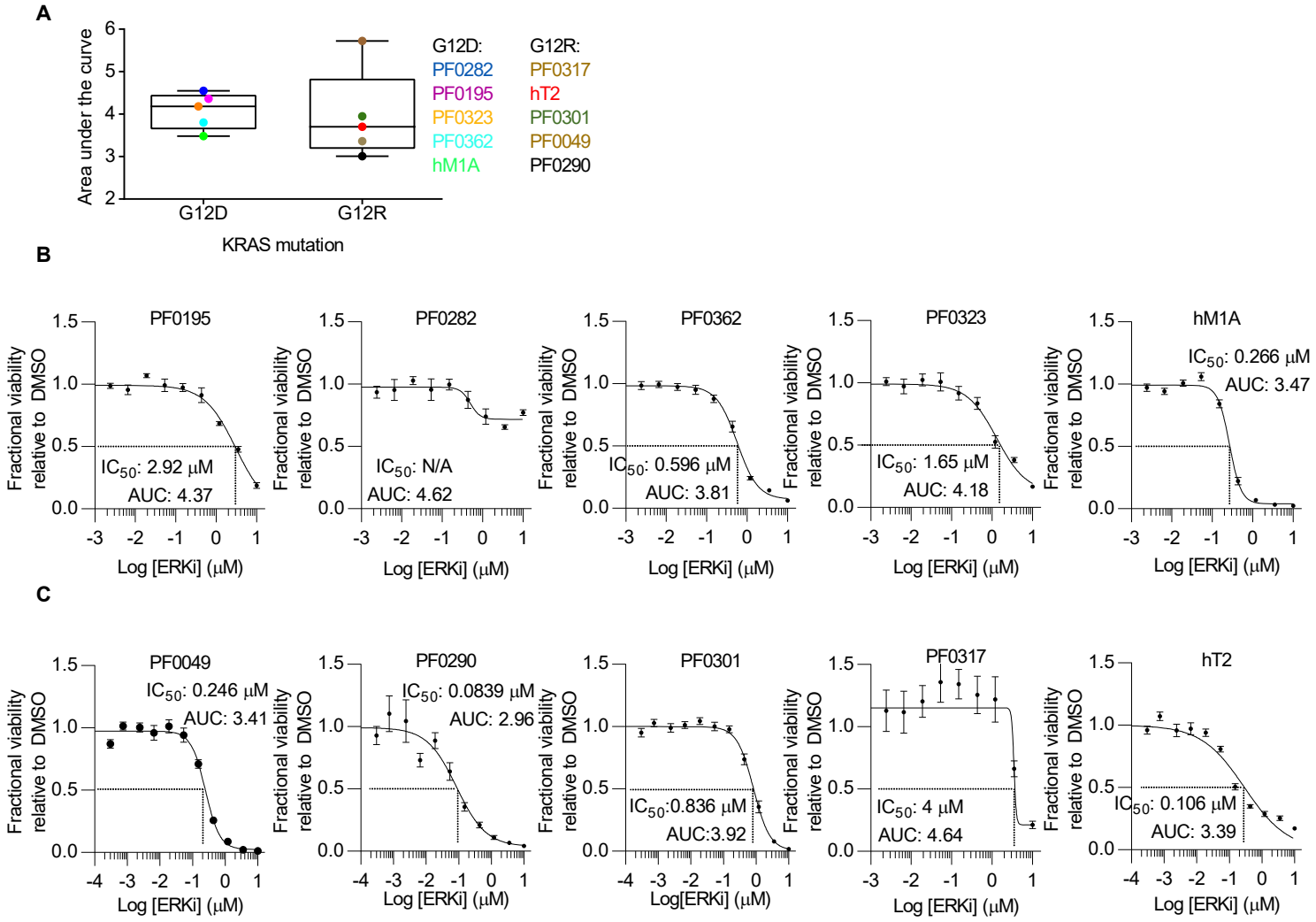

Figure S7. KRAS^{G12R} organoids are sensitive to ERK MAPK inhibition.
A, Plot of the area under the curve for KRAS^{G12D}- and KRAS^{G12R}-mutant pancreas cancer organoids. AUC calculated from three independent experiments. The difference was not significant. **B,** Cell viability curves of KRAS^{G12D}-mutant organoids treated with ERKi for 10 days. Data are the average of three independent experiments. **C,** Cell viability curves of KRAS^{G12R}-mutant organoids treated with ERKi for 10 days. Data are the average of three independent experiments.

Supplementary Fig. S8

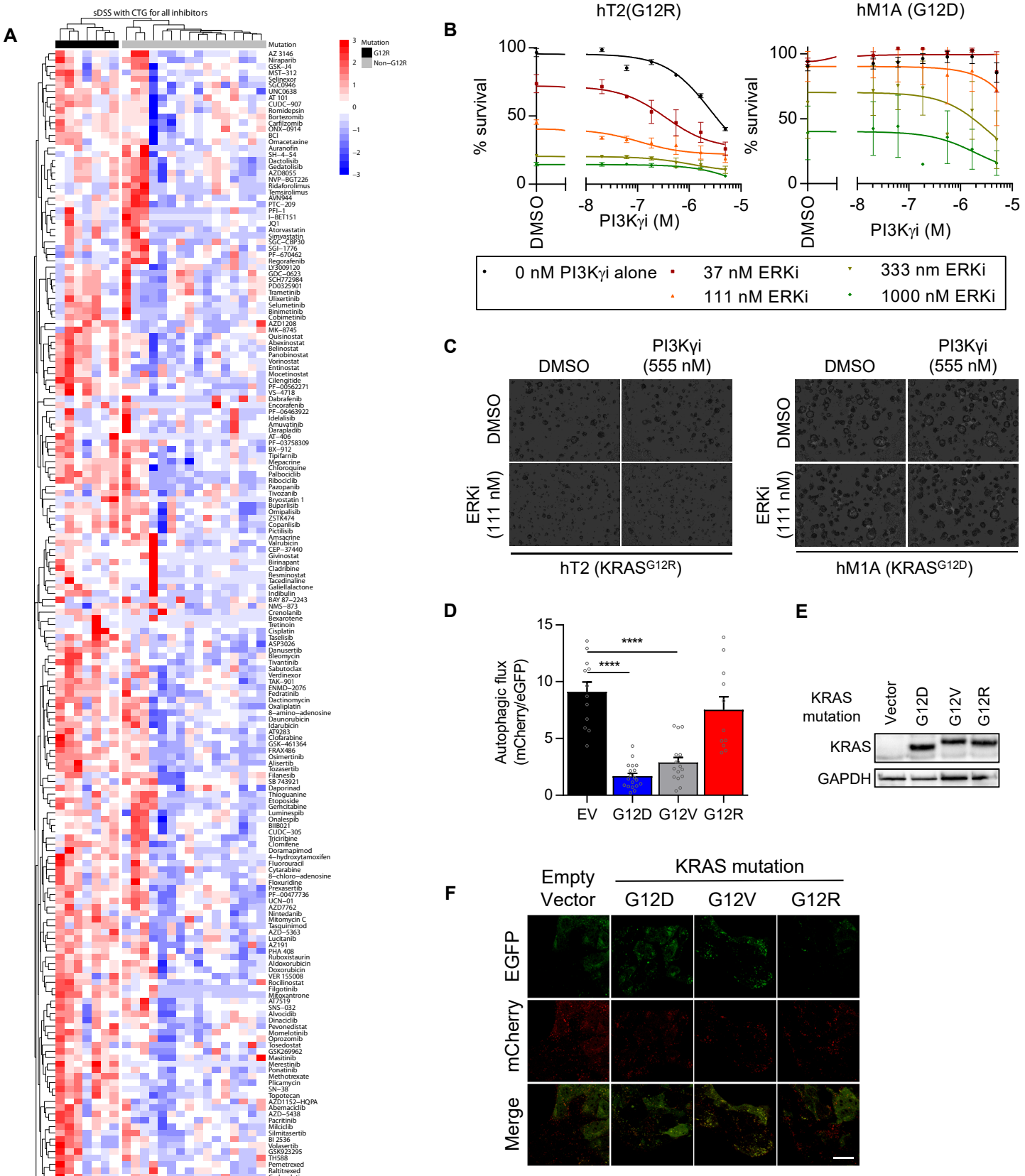

Figure S8. $KRAS^{G12R}$ PDAC cell lines are fundamentally different from non$KRAS^{G12R}$ cell lines. **A**, 525-drug sensitivity and resistance testing of multiple PDAC cell lines expressing $KRAS^{G12R}$ and other KRAS mutations. Cell viability was measured using cell titer glo and response to each inhibitor was averaged and ranked according to its deviation from the average. Data are an average of three independent experiments. **B**, Cell viability of PDAC organoid cultures co-treated with ERKi (SCH772984) and PI3Kγi (IPI-549). Organoids were cultured for 10 days. Data are the average of two independent experiments. **C**, Bright field images from **B**. Right, hT2 ($KRAS^{G12R}$); left, hM1A ($KRAS^{G12D}$). **D**, Ectopic expression of $KRAS^{G12R}$ in RIE-1 cells dos not suppress autophagy. RIE-1 cells were transduced to stably express KRAS and mCherry-EGFP-LC3B. Autophagic index indicates the ratio of the areas of $mCherry^{+}$ punctae to $EGFP^{+}$ punctae. Mean autophagic index is plotted, with each individual data point representing one field containing at least five analyzed cells. Data are representative of three independent experiments. (***P<0.0002, **P<0.0021, *P<0.032, p values from Dunnett's multiple comparison test after one-way ANOVA, comparing all lanes to EV). Error bars, mean ± s.e.m. **E**, Immunoblot analysis of KRAS-expressing RIE-1 cells used in **A**. **F**, Representative confocal images of EGFP, MCHERRY and merged channels used to quantify the autophagic index, used in **D**. For **D-F**, EV and G12V were previously reported (1).

1. Bryant KL, Stalnecker CA, Zeitouni D, Klomp JE, Peng S, Tikunov AP, et al. Combination of ERK and autophagy inhibition as a treatment approach for pancreatic cancer. Nat Med 2019;25:628-40.